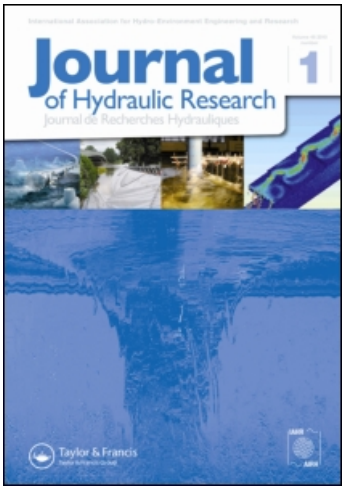

Journal of Hydraulic Research
Publication details, including instructions for authors and subscription information:
http://www.informaworld.com/smpp/title~content=t916282780

Hydrodynamic instability of hyperconcentrated flows of the Yellow River

Yuchuan Bai[a]; Haijue Xu[a]
[a] Institute for Sedimentation on River and Coastal Engineering, Tianjin University, Tianjin, People's Republic of China

Online publication date: 13 December 2010

To cite this Article Bai, Yuchuan and Xu, Haijue(2010) 'Hydrodynamic instability of hyperconcentrated flows of the Yellow River', Journal of Hydraulic Research, 48: 6, 742 — 753
To link to this Article: DOI: 10.1080/00221686.2010.515384
URL: http://dx.doi.org/10.1080/00221686.2010.515384

Journal of Hydraulic Research Vol. 48, No. 6 (2010), pp. 742–753
doi:10.1080/00221686.2010.515384

Research paper

Hydrodynamic instability of hyperconcentrated flows of the Yellow River

YUCHUAN BAI, Professor, *Institute for Sedimentation on River and Coastal Engineering, Tianjin University, Tianjin 300072, People's Republic of China.*
Email: ychbai@tju.edu.cn (author for correspondence)

HAIJUE XU, Associate Professor, *Institute for Sedimentation on River and Coastal Engineering, Tianjin University, Tianjin 300072, People's Republic of China.*
Email: xiaoxiaoxu_2004@163.com

ABSTRACT
Sediment concentrations of Chinese rivers are among the highest worldwide. If the sediment concentration exceeds a certain value, the flow dramatically changes exhibiting properties different from low-concentration sediment-laden flows, both in the movement and the pattern of sediment transportation. The hyperconcentrated flow exhibits distinct phenomena, such as "instability flow", "clogging river", or "blast flow". Such flow phenomena are related to the formation, development and break-up of a hyperconcentrated laminar layer, and also reflect the transition from laminar to turbulent and return to laminar flow. The turbulence intensity of the hyperconcentrated flow is normally weak with turbulence largely damped as the sediment concentration becomes sufficiently high. It was found that the instability of hyperconcentrated flows is not only controlled by the critical Reynolds number, but also related to sediment concentration, distribution of the sediment in water, and the size and density of the sediment particles.

Keywords: Hyperconcentrated flow, instability, sediment motion, turbulence, Yellow River

1 Introduction

Rivers in China discharge sediments at a huge rate, a well-known example being the Yellow River. During flood season, its sediment concentration is typically 300 kg/m^3. In some of its mid-reaches, the sediment concentration can be as high as 1500 kg/m^3. Historical data revealed that the sediment carried by the floods has a large impact on the erosion and sedimentation processes. These floods occur frequently in the Yellow River and along its tributaries on the Loess Plateau. For example, among the forty-two flood peaks recorded at the Beiluo branch of the Yellow River from 1964 to 1978, there were 27, 7 and 8 of them in which the maximum daily-averaged sediment concentration was, respectively, larger than 500 kg/m^3, in the range of 100–500 kg/m^3, and less than 100 kg/m^3, with a suspended load of approximately 66, 7, and 3% of the total sediment load, respectively.

Although there is no standard definition, a flow is termed hyperconcentrated if the fine sediment content reaches a certain level. A water–sediment mixture becomes hyperconcentrated if the fine particles of a diameter less than 0.01 mm represent for a certain fraction by sediment weight so that it can no longer be described as a Newtonian fluid. Sediments washed from the Loess Plateau are fine in the south and relatively coarse in the north, with median diameters from 0.005 to 0.1 mm. The sediment carrying capacity of a hyperconcentrated current is extremely high, and the sediment is transported as wash load. The highest sediment concentration measured on the Loess Plateau is above 1600 kg/m^3 (Wan and Wang 1994).

The hyperconcentrated water flow has distinct phenomena, including the so-called "flow induced threads", "blast flow or instability flow", and "clogging river". Flows with a high sediment concentration can be laminar, with a thin layer of clear water on the surface where thread-like stream filaments are visible, referred to as "flow induced threads". If the white powder is spread along a straight line across the flow surface, the line keeps its form without mixing, as it moves with the fluid. Observations revealed an unsheared "plug flow" in the central river portion. This "plug flow" extends vertically downward from the free surface almost to the bed (Qian 1989).

If the current intensity is weak, there is usually a layer of stagnant turbid water near the river bed, which is not in a solid state

Revision received 4 August 2010/Open for discussion until 30 June 2011.

ISSN 0022-1686 print/ISSN 1814-2079 online
http://www.informaworld.com

but keeps the fluidity. As the stagnant layer develops, the water level rises correspondingly. The growth of this layer and the increase of the water level mainly occur in the middle and upper reaches, causing the water surface profile to become steeper and the velocity to increase. The stagnant layer continues to thicken until it disintegrates abruptly, causing a sudden drop in the water level, flattening of the water surface, and velocity reduction. Then a new stagnant layer is developed, and the cycle repeats itself. A full cycle consists of gradual rising and abrupt reduction of the water surface, referred to as the "blast flow" or "instability flow".

As the sediment concentration exceeds a certain threshold, the flood discharge and flow velocity may drop abruptly, causing the flow to stop completely, and become locally stagnant. This type of in hyperconcentrated flow blockage is known as "clogging".

The above phenomena reduce to a stability problem of hyperconcentrated flow, which is controlled by the flow transition from laminar to turbulent and then back to the laminar state. For concentrations exceeding a certain critical value, the effect increases strongly with concentration. Given that a hyperconcentrated fluid has a much higher bulk density than a normal fluid, the flow may locally or temporally relaminarize from turbulence, leading to "flow-induced threads" and "clogging" phenomena. These flows can sustain a higher velocity without turbulence, with a critical Reynolds number varying between 2000 and 10^5.

The relationship between sediment concentration and turbulence strength is complex. A reduction of sediment concentration may result in a decrease of the viscosity coefficient, which in turn will intensify the turbulent strength, thereby enhancing the capability of the flow to carry more sediment. These changes end up in an increase of sediment concentration, by which an opposite phase of the cycle is initiated leading to a decrease in the sediment-carrying capacity. Therefore, there is a cyclic increase and decrease in sediment concentration. In a smooth channel, the wall resistance increases dramatically as the flow changes from laminar to turbulent, and vice versa. As a result, these time-periodical flow variations are more conspicuous in a smooth channel, with a large-amplitude periodic rise and drop of the water surface, namely the appearance of blast flow.

The characteristics of the hyperconcentrated flow were studied by Qian (1989) who described the development, flocculation, rheology, hydraulics, and applications of hyperconcentrated flows. Julien (1989), Julien and Lan (1991), and O'Brien and Julien (1995) conducted laboratory studies on the physical properties and mechanics of hyperconcentrated flows. Wang and Qian (1985), Wang *et al.* (1994, 1998) and Wang (2002) described the rheological properties of these flows, and the mechanisms of surface instability and drag reduction.

Different from the usual hyperconcentrated flows, the exceptionally large sediment concentration and the wide particle size grading of the Yellow River greatly influence the flow characteristics. Wan and Wang (1994) described the mechanisms of ripping-up-the-bottom, river clogging, roll waves, and instability of the hyperconcentrated flow. Qian *et al.* (1985) and Chien *et al.* (1998) discussed qualitatively the transition from laminar to turbulent flow, and the instability phenomena in the Yellow River. Qian (1989) and Fei (1994) discussed the viscosity variation of hyperconcentrated flow as a function of sediment concentration and concentration distribution, comparing the results with observations.

A theoretical analysis on the stability of Newtonian fluid flows was made in the early 1970s. Semi-empirical relations for the transition from laminar to turbulent flows include ore tailings (Hanks 1963, Wasp 1977, Abulnaga 2002, Alderman and Haldenwang 2007). Results of the linear stability analysis were reported for plane and circular Poiseuille closed conduit flow. Frigaard *et al.* (1994) and Frigaard and Nouar (2003) performed two-dimensional (2D) and nonlinear three-dimensional (3D) perturbation analyses with the results depending on the Bingham number. Phenomenological and theoretical results were also compared by Nouar and Frigaard (2001).

This research aims to study the instability of hyperconcentrated flows with particular emphasis on conditions pertinent to the Yellow River, and to provide theoretical explanations to the interesting field phenomena. Results derived herein can be used as a theoretical basis to guide the development of diversion works in irrigated areas and the optimal design of irrigation channels.

2 Governing equations for hyperconcentrated flows

2.1 *Basic equations*

Consider a coordinate system made up by $x =$ streamwise coordinate, $z =$ transverse coordinate, and $y =$ upward and normal to the x–z plane. $J = \sin\theta$ is bottom slope. Then, the continuity equation for mass conservation is

$$\frac{\partial(1-C)}{\partial t}+\frac{\partial(1-C)u}{\partial x}+\frac{\partial(1-C)v}{\partial y}+\frac{\partial(1-C)w}{\partial z}=0 \quad (1)$$

The momentum equations can be written as

$$\frac{\partial(1-C)u_i}{\partial t}+\frac{\partial(1-C)u_ju_i}{\partial x_j}=(1-C)g_i-\frac{1}{\rho}(1-C)\frac{\partial p}{\partial x_i}-\frac{F_i}{\rho}+\frac{(1-C)}{\rho}\frac{\partial \tau_{ji}}{\partial x_j} \quad (2)$$

where u_i ($i = 1,2,3$) = velocity components in the x, y and z directions, respectively, and $p =$ pressure, $C =$ the volume concentration of sediment, $g =$ gravity, and $\tau_{ij} =$ stress components of the flow. Further $F_i =$ force acting between sediment particles and water, including the drag due to viscosity and the pressure gradient, and buoyancy induced by gravity (Kobayashi and Seo 1985). Its three components along the x, y and z directions

are

$$\begin{cases} F_x = -C\rho g \sin\theta + \frac{1}{2}\rho C_D C_2 d^2 \sqrt{u_r^2 + v_r^2 + w_r^2} \cdot u_r \cdot n_s \\ F_y = C\rho g \cos\theta + \frac{1}{2}\rho C_D C_2 d^2 \sqrt{u_r^2 + v_r^2 + w_r^2} \cdot v_r \cdot n_s \\ F_z = \frac{1}{2}\rho C_D C_2 d^2 \sqrt{u_r^2 + v_r^2 + w_r^2} \cdot w_r \cdot n_s \end{cases} \tag{3}$$

in which C_D = drag coefficient, d = sediment diameter, C_2 = area coefficient of sediment particles, $n_s = C/C_3 d^3$ = number of particles per unit volume, C_3 = volume coefficient of particles, and u_r, v_r and w_r = relative (subscript r) velocities between water and sediment particles (u_s, v_s and w_s) along the x, y and z directions, i.e.

$$\begin{cases} u_r = u - u_s \\ v_r = v - v_s \\ w_r = w - w_s \end{cases} \tag{4}$$

The drag coefficient C_D is considered identical as for a single particle settling in still water, $C_D = 2C_3/C_2 \times (s-1)gd/\omega^2$, where ω = settling velocity and $s = \rho_s/\rho$ = relative sediment density. Substituting Eq. (4) into Eq. (3), and using the two above expressions, the forces acting between sediment particles and water are

$$\begin{cases} F_x = C\rho g\left[-\sin\theta + (s-1)\sqrt{u_r^2 + v_r^2 + w_r^2}\,\frac{u_r}{\omega^2}\right] \\ F_y = C\rho g\left[\cos\theta + (s-1)\sqrt{u_r^2 + v_r^2 + w_r^2}\,\frac{v_r}{\omega^2}\right] \\ F_z = C\rho g\left[(s-1)\sqrt{u_r^2 + v_r^2 + w_r^2}\,\frac{w_r}{\omega^2}\right] \end{cases} \tag{5}$$

Assuming that the sediment particles follow closely the flow, and the relative velocity is only caused by the sediment settling, then (Qian *et al.* 1985)

$$\begin{cases} u_s = \omega \sin\theta + u \\ v_s = -\omega \cos\theta + v \\ w_s = w \end{cases} \tag{6}$$

Further, from Eqs. (4)–(6),

$$\begin{cases} F_x = C\rho g[-\sin\theta + (s-1)(-\sin\theta)] \\ \quad = -C\rho g s \sin\theta = -C\rho_s g \sin\theta \\ F_y = C\rho g[\cos\theta + (s-1)\cos\theta] = C\rho g s \cos\theta = C\rho_s g \cos\theta \\ F_z = 0 \end{cases} \tag{7}$$

2.2 *Determination of internal stress*

The sediment in the Yellow River mainly originates from its middle reaches, where the grain size is increasingly fine from northwest ($d > 0.045$ mm) to southeast with $d < 0.015$ mm. The grain size composition has obvious zonal distribution characteristics (Fig. 1). The data show that the flow in the coarse sediment area has a higher sediment concentration, often larger than 1000 kg/m^3. High sediment concentration has a significant effect on water viscosity, greatly reducing the settling velocity of coarse sediment and therefore enhancing the carrying capacity with the coarse particles.

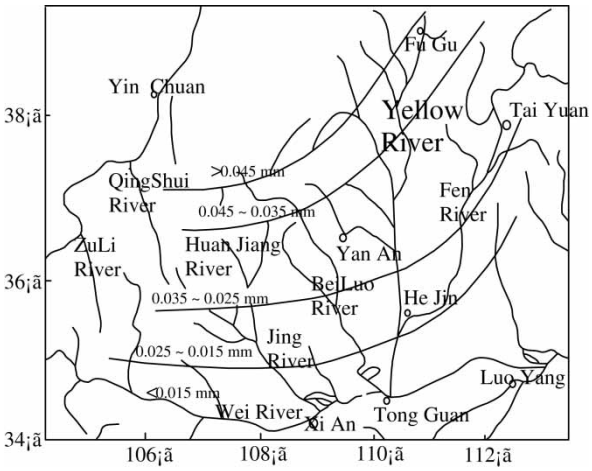

Figure 1 Variation of medium sediment diameter in middle reach of Yellow River (Zhao *et al.* 1997)

2.2.1 *Generalized viscosity model*

Because of the inter-particle interactions as well as the interactions between particles and water, hyperconcentrated flows follow a non-Newtonian constitutive relation as

$$\tau = \tau_B + k\left(\frac{\mathrm{d}u}{\mathrm{d}y}\right)^m = \tau_B + \mu\frac{\mathrm{d}u}{\mathrm{d}y}, \tag{8}$$

in which τ_B = Bingham yield stress, and $\mu = (\mathrm{d}u/\mathrm{d}y)^{m-1}$ = generalized viscosity, studied for the hyperconcentrated river flow by Qian (1989) and Fei (1994). These flows can be classified into three categories, in terms of concentration by mass of particles with $d < 0.01$ mm.

(1) No cohesive particles in the water column (measured in terms of particles with $d < 0.01$ mm): because of the weak physical–chemical effects between particles, the effects of bound water on the effective concentration can be neglected and no fine particulates are considered. Therefore, the fluid remains Newtonian as long as the sediment concentration is not very high. The relative viscosity of suspension is (Roscoe 1952 or Thomas 1965)

$$\frac{\mu}{\mu_0} = (1 - 1.35C)^{-2.5} \tag{9a}$$

(2) Mass concentration of cohesive particles ($d < 0.01$ mm) is more than 15%. Then the particles are mainly silt or clay, and the hyperconcentrated flow with these fine particles often exhibits non-Newtonian characteristics. With an increase of sediment concentration, an aggregate structure is

usually formed. Taking into account the increased volume due to an absorbed film of water, the effective concentration coefficient is (Fei and Yang 1985)

$$K' = 1 + 6\sum \frac{p_i}{D_i}\delta_i + \frac{k'\sigma}{1-\sigma} \tag{9b}$$

in which the second term represents the contribution of the absorbed water volume to the effective concentration, and the third term is due to occlusion water. If the concentration of the suspension is very high, then $k' \approx 0$. This model accounts for the relative stiffness coefficient of the fine particle suspension as

$$\mu = \left(1 - k \cdot \frac{C}{C_{Vm}}\right)^{-2.5} \tag{9c}$$

with $k = 1 + (3/2) \times [(C_{Vm} - C)/C_{Vm}]^4$ = modification of effective concentration coefficient due to occlusion water, based on rheological tests of tens of different grain sizes and concentrations of suspended load sampled in the middle and lower reaches of the Yellow River, resulting for the relative viscosity coefficient in

$$\frac{\mu}{\mu_0} = \left\{1 - \left[1 + \frac{3}{2}\left(\frac{C_{Vm} - C}{C_{Vm}}\right)^4\right]\frac{C}{C_{Vm}}\right\}^{-2.5} \tag{10}$$

in which μ_0 = viscosity coefficient of clear water, $C_{Vm} = 1/K' = 1/\sum(1 + 6\delta\Delta p_i/d_i)$ with subscript m = critical concentration taking into account the effect of sediment gradation on suspension viscosity, K' = effective concentration coefficient, δ = thickness of the pellicular zone, d_i = diameter of ith sediment and Δp_i = percentage of ith sediment. Note from Fig. 2 that the results obtained from Eq. (10) agree well with the test data.

The Bingham shear stress τ_B for the hyperconcentrated flow was studied by Bai *et al.* (2002). If the concentration of fine particles is low, τ_B can be neglected. However, if the concentration of fine particles by weight is >10%, the sediment–water mixture exhibits non-Newtonian properties, such that

$$\tau_B = 9.8 \times 10^{-2} \exp(B\varepsilon + 1.5) \tag{11}$$

in which parameter $B = 8.45$, $\epsilon = (C - C_{V0})/C_{Vm}$, where C_{V0} = initial (subscript 0) concentration (Fig. 3).

(3) If the particle composition is widely distributed with a low portion of cohesive particles, then the flow concentration in coarse sediment areas in the middle reaches of the Yellow River is higher than 1000 kg/m^3, with the coarsest grains larger than $d = 1$ mm. Its pores are filled with finer particles, and the coarse particles are surrounded by a bound water layer, which does not affect the critical concentration C_{Vm}. Hence, it is reasonable to heat the sample in water, and to wait for precipitation until the solid volume is steady, such that the measured volume concentration equals the critical concentration. The viscosity of the suspension is calculated using Eq. (10).

2.2.2 *Equivalent viscosity coefficient model*

In practice, the equivalent viscosity model was adopted for the Yellow River as

$$\tau = \mu_e \frac{\mathrm{d}u}{\mathrm{d}y} \tag{12}$$

in which $\mu_e = \tau_B/(\mathrm{d}u/\mathrm{d}y) + k(\mathrm{d}u/\mathrm{d}y)^{m-1}$, related to the sediment concentration. Sha (1961) studied the viscosity of hyperconcentrated flows, suggesting the concept of the stagnant limit concentration C_0. If $C/C_0 = 1$, $\mu_0/\mu = 0$ and $\mu = \infty$, the characteristics of turbid water change, and do not follow the viscous flow behaviour. Therefore, C_0 is a function of the sediment diameter thickness ratio d/δ. If the water film thickness $\delta \approx 0.0001$ mm, then

$$\mu_e = \mu_0\left(1 - \frac{C}{2(d_{50})^{1/2}}\right)^{-1} \tag{13}$$

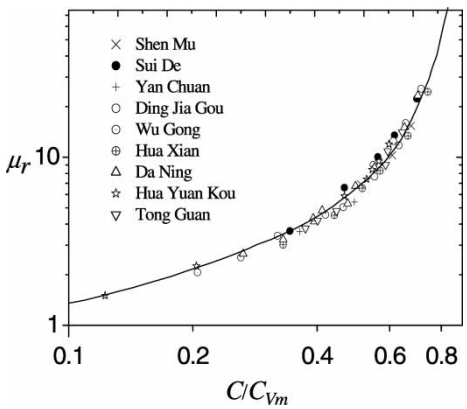

Figure 2 Relationship $\mu_r[C/C_{Vm}]$, (– –) Eq. (10)

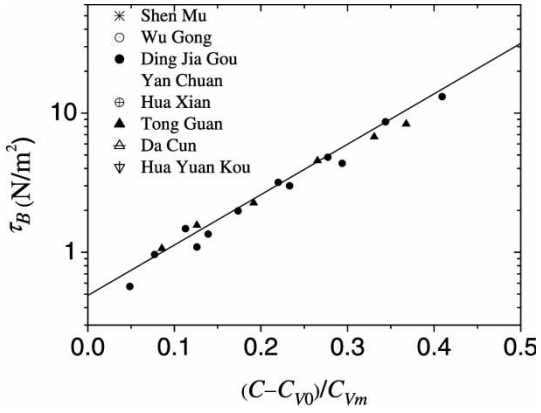

Figure 3 $\tau_B[(C - C_{V0})/C_{Vm}]$ of middle and lower Yellow River reaches, with (– –) Eq. (11)

Taking the Bingham shear stress into account, the relationship between the shear stress and shear rate is

$$\tau_{ij} = 2\mu_e S_{ij} \tag{14}$$

in which $\mu_e = \mu + \tau_B/II (II = (1/2 \times S_{ij} \cdot S_{ij})^{1/2})$ = generalized viscosity. Because the Bingham shear stress does not play a role in viscous motion, the relationship between viscosity of clear and turbid water is

$$F(C) = \left(1 - \frac{C}{2(d_{50})^{1/2}}\right) \tag{15}$$

3 Flow stability of hyperconcentrated flows

3.1 *Normalized equations*

To normalize the governing equations, consider $U = u/u_m$, $V = v/u_m$, $W = w/u_m$, $P = p/\rho {u_m}^2$, where u_m = maximum (subscript m) velocity on the surface, h the water flow depth, C = volumetric sediment concentration. Introducing the Froude number $\mathsf{F} = u_m/(gh)^{1/2}$, and the Reynolds number $\mathsf{R} = \rho {u_m}^2 h/\mu_E$, the normalized governing equations read

$$\frac{\partial(1-C)}{\partial t} + \frac{\partial(1-C)U}{\partial x} + \frac{\partial(1-C)V}{\partial y} + \frac{\partial(1-C)W}{\partial z} = 0 \tag{16}$$

$$\frac{\partial(1-C)U}{\partial t} + \frac{\partial(1-C)UU}{\partial x} + \frac{\partial(1-C)UV}{\partial y} + \frac{\partial(1-C)UW}{\partial z} = \frac{(1-C)}{\mathsf{F}^2}\sin\theta - (1-C)\frac{\partial P}{\partial x} + C\frac{\rho_s}{\rho}\frac{1}{\mathsf{F}^2}\sin\theta + (1-C) \times \left[\frac{1}{\mathsf{R}}\nabla^2 U + \frac{1}{\mathsf{R}}\frac{\partial}{\partial x}\left(\nabla\cdot\vec{U}\right) + \frac{\partial}{\partial y}\left(\frac{1}{\mathsf{R}}\right)\left(\frac{\partial U}{\partial y} + \frac{\partial V}{\partial x}\right)\right] \tag{17}$$

$$\frac{\partial(1-C)V}{\partial t} + \frac{\partial(1-C)UV}{\partial x} + \frac{\partial(1-C)VV}{\partial y} + \frac{\partial(1-C)VW}{\partial z} = -\frac{(1-C)}{\mathsf{F}^2}\cos\theta - (1-C)\frac{\partial P}{\partial y} - C\frac{\rho_s}{\rho}\frac{1}{\mathsf{F}^2}\cos\theta + (1-C)\left[\frac{1}{\mathsf{R}}\nabla^2 V + \frac{1}{\mathsf{R}}\frac{\partial}{\partial y}\left(\nabla\cdot\vec{U}\right) + 2\frac{\partial}{\partial y}\left(\frac{1}{\mathsf{R}}\right)\frac{\partial V}{\partial y}\right] \tag{18}$$

$$\frac{\partial(1-C)W}{\partial t} + \frac{\partial(1-C)UW}{\partial x} + \frac{\partial(1-C)VW}{\partial y} + \frac{\partial(1-C)WW}{\partial z} = -(1-C)\frac{\partial P}{\partial z} + (1-C) \times \left[\frac{1}{\mathsf{R}}\nabla^2 W + \frac{1}{\mathsf{R}}\frac{\partial}{\partial z}\left(\nabla\cdot\vec{U}\right) + \frac{\partial}{\partial y}\left(\frac{1}{\mathsf{R}}\right)\left(\frac{\partial W}{\partial y} + \frac{\partial V}{\partial z}\right)\right] \tag{19}$$

Both velocities and the pressure may be decomposed into a time-averaged, and a fluctuating term. Substituting into Eqs. (16)–(19) and imposing the associated boundary conditions, the governing equations and boundary conditions for the base flow and the fluctuating flow are as follows.

3.2 *Solution for base flow of hyperconcentrated channel flow*

Consider steady uniform flow subject to the boundary conditions $u_b(y=0) = 0$, $p_b(y=1) = p_0$, and $\partial u_b/\partial y(y=1) = 0$. Taking into account Eq. (15), the velocity distribution for the base flow is

$$u_b = -\frac{\sin\theta}{\mathsf{F}^2}\int_0^y \mathsf{R}\left(\int_1^y \frac{\rho_a}{1-C}\mathrm{d}y + C_2\right)\mathrm{d}y + C_3 \tag{20}$$

in which the constants of integration are $C_2 = C_3 = 0$. If the distribution of the suspension concentration is determined, the velocity distribution is known as well. If the distribution of the suspension concentration is at equilibrium, the diffusion equation can be simplified to

$$\varepsilon_y \frac{\mathrm{d}C}{\mathrm{d}y} + C\omega = 0 \tag{21}$$

(1) If the diffusion coefficient ϵ_y = constant, the solution of Eq. (21) is

$$\frac{C}{C_a} = \mathrm{e}^{-\omega(y-a)/\varepsilon_y} = \mathrm{e}^{-s(y-a)} \tag{22}$$

in which a = dimensionless thickness of the bed load, ω = dimensionless sediment settling velocity, ε_s = dimensionless sediment dispersion coefficient, and C_a = reference concentration. The effects of sediment diffusion and settlement are accounted for by the sediment suspension index $\zeta = \omega/\varepsilon_s$. Hurst (1929) mixed water with various sediment sizes, and found that the measured distribution was closely described by Eq. (22). Lane and Kalinske (1941) investigated the data based on natural sediments, and observed that Eq. (22) can serve well for practical purposes.

(2) If ε_y = momentum exchange coefficient, and the logarithmic velocity distribution is adopted, then

$$\frac{C}{C_a} = \left(\frac{h-y}{y}\frac{a}{h-a}\right)^Z \tag{23}$$

By accounting for the effect of sediment concentration on the settling velocity, the latter is for the Yellow River

$$\omega = \omega_0\left(1 - \beta_c \bar{C}\right)^m \tag{24}$$

where $\beta_c = 1.77$, $m = 2.5$, $\bar{C}$ = mean concentration, and ω_0 = sediment settling velocity in clear water. The sediment distribution is determined by the suspension index Z. To verify Eq. (23), Qian (1989) measured the concentration distribution whose average concentrations were 270, 421, and 963 kg/m^3,

respectively, in the Dingjiagou station of the Wuding River, a branch of the Yellow River. From the relation $C \sim (h - y)/y$, he discovered that the results given by Eq. (23) agree well with the concentration distribution of the Yellow River. Also, among all sediment sizes, these with the higher concentration had an even distribution.

According to the analytical results, two sediment concentration distribution are adopted.

(a) Uniform sediment concentration, $\partial C/\partial y = 0$. Introducing the dimensionless turbid water density, $\rho_a = (1 - C) + \rho_s/\rho \times C = 1 + (\rho_s - \rho)C/\rho$, the velocity distribution for the base flow obtains

$$u_b = \frac{1}{1-C}\frac{\rho_a}{2}\frac{\mathrm{R}}{\mathrm{F}^2}\left(2y - y^2\right)\sin\theta \tag{25}$$

and the maximum velocity

$$U_m = \frac{g}{2\nu}\left(1 + \frac{C}{1-C}\frac{\rho_s}{\rho}\right)\sin\theta \cdot h^2 \tag{26}$$

(b) For a non-uniform sediment concentration $\partial C/\partial y \neq 0$, using Eq. (15) and integrating, the expression for velocity is

$$\begin{aligned} u_b(y) = {} & \frac{\mathrm{R}_0 \sin\theta}{\mathrm{F}^2}\left\{-B_1\left[y - \frac{C_a}{2(d_{50})^{1/2}}\left(-\frac{\varepsilon_y}{\omega}\right)\mathrm{e}^{-\omega(y-a)/\varepsilon_y}\right] - \frac{y^2}{2}\right. \\ & - \frac{C_a}{2(d_{50})^{1/2}}\frac{\varepsilon_y}{\omega}y \cdot \mathrm{e}^{-\omega(y-a)/\varepsilon_y} - \frac{C_a}{2(d_{50})^{1/2}}\left(\frac{\varepsilon_y}{\omega}\right)^2 \cdot \mathrm{e}^{-\omega(y-a)/\varepsilon_y} \\ & - \frac{\rho_s}{\rho}\frac{\varepsilon_y}{\omega}\left[\int \ln\left[1 - C_a\mathrm{e}^{-\omega(y-a)/\varepsilon_y}\right]\mathrm{d}y\right. \\ & - \frac{1}{2(d_{50})^{1/2}}\left(-\frac{\varepsilon_y}{\omega}\right)\left\{C_a \cdot \mathrm{e}^{-\omega(y-a)/\varepsilon_y} \cdot \ln\left(1 - C_a\mathrm{e}^{-\omega(y-a)/\varepsilon_y}\right)\right. \\ & \left.\left.\left. - C_a \cdot \mathrm{e}^{-\omega(y-a)/\varepsilon_y} - \ln\left(1 - C_a \cdot \mathrm{e}^{-\omega(y-a)/\varepsilon_y}\right)\right\}\right]\right\} \\ & + B_2 \end{aligned} \tag{27}$$

in which

$$B_1 = 1 + \frac{\rho_s}{\rho}\frac{\varepsilon_y}{\omega}\ln\left[1 - C_a \cdot \mathrm{e}^{-\omega(y-a)/\varepsilon_y}\right] \quad \text{and}$$

$$\begin{aligned} B_2 = {} & \frac{\mathrm{R}_0 \sin\theta}{\mathrm{F}^2}\left\{-B_1\frac{C_a}{2(d_{50})^{1/2}}\left(-\frac{\varepsilon_y}{\omega}\right)\mathrm{e}^{-\omega(0-a)/\varepsilon_y} + \frac{C_a}{2(d_{50})^{1/2}}\right. \\ & \left. \times \left(\frac{\varepsilon_y}{\omega}\right)^2 \mathrm{e}^{-\omega(0-a)/\varepsilon_y}\right. \\ & + \frac{\rho_s}{\rho}\frac{\varepsilon_y}{\omega}\left[-\frac{1}{2(d_{50})^{1/2}}\left(-\frac{\varepsilon_y}{\omega}\right)\left\{C_a \cdot \mathrm{e}^{-\omega(0-a)/\varepsilon_y} \cdot \ln\left(1 - C_a \cdot \mathrm{e}^{-\omega(0-a)/\varepsilon_y}\right)\right.\right. \\ & \left.\left. - C_a \cdot \mathrm{e}^{-\omega(0-a)/\varepsilon_y} - \ln\left(1 - C_a \cdot \mathrm{e}^{-\omega(0-a)/\varepsilon_y}\right)\right\}\right]\Big\} \end{aligned}$$

3.3 *Disturbance equation of hyperconcentrated channel flow*

The variation of flow velocity is a direct cause of the flow instability, and the variation in sediment concentration is caused by the variation of flow velocity. Consequently, in stability analysis, the instability induced by velocity fluctuations is only considered, but not the fluctuation in sediment concentration, i.e. $C' = 0$. The fluctuating terms may be defined with $\theta = \alpha_b x + \beta z - \omega_b t$ as

$$\begin{pmatrix} u' \\ v' \\ w' \\ p' \end{pmatrix} = \begin{pmatrix} \hat{u}_{ob}(y) \\ \hat{v}_{ob}(y) \\ \hat{w}_{ob}(y) \\ \hat{p}_{ob}(y) \end{pmatrix} e^{i\theta} \tag{28}$$

Substituting Eq. (28) for the fluctuating terms (u', v', w') in Eqs. (16)–(19), the Orr-Sommerfeld (O-S) equation for the fluctuating terms in hyperconcentrated flows results with $\mathrm{D} = \mathrm{d}/\mathrm{d}y$

$$\begin{aligned} & \left\{\left[\mathrm{D}^2 - \left(\alpha_b^2 + \beta^2\right)\right]^2 - i\mathrm{R}(\alpha_b u_b - \omega_b)\left[\mathrm{D}^2 - \left(\alpha_b^2 + \beta^2\right)\right] + i\alpha_b \mathrm{R}\frac{\mathrm{d}^2 u_b}{\mathrm{d}y^2}\right\}\hat{v}_{0b} \\ & - \left\{\mathrm{D}^2 - \left(\alpha_b^2 + \beta^2\right) - i\mathrm{R}(\alpha_b u_b - \omega_b)\right\} \\ & \quad \times \left[-\hat{v}_{0b}\frac{\mathrm{d}^2}{\mathrm{d}y^2}\ln(1-C) - \frac{\mathrm{d}\hat{v}_{0b}}{\mathrm{d}y}\frac{\mathrm{d}\ln(1-C)}{\mathrm{d}y}\right] \\ & + i\mathrm{R}\alpha_b\frac{\mathrm{d}u_b}{\mathrm{d}y}\left[-\hat{v}_{0b}\frac{\mathrm{d}\ln(1-C)}{\mathrm{d}y}\right] + \frac{\mathrm{d}}{\mathrm{d}y}(\ln \mathrm{R}) \\ & \quad \cdot \mathrm{D}\left[\left(\alpha_b^2 + \beta^2\right) - \mathrm{D}^2\right]\hat{v}_{0b} \\ & + \left[\frac{\mathrm{dR}}{\mathrm{d}y}i(\alpha_b u_b - \omega_b) + \frac{\mathrm{d}^2}{\mathrm{d}y^2}(\ln \mathrm{R}) \cdot \mathrm{D}\right] \\ & \quad \times \left[-\frac{\mathrm{d}\hat{v}_{0b}}{\mathrm{d}y} - \hat{v}_{0b}\frac{\mathrm{d}\ln(1-C)}{\mathrm{d}y}\right] \\ & - \left[\frac{\mathrm{d}}{\mathrm{d}y}\ln \mathrm{R} \cdot \mathrm{D}\right]\left[\hat{v}_{0b}\frac{\mathrm{d}^2\ln(1-C)}{\mathrm{d}y^2} + \frac{\mathrm{d}\hat{v}_{0b}}{\mathrm{d}y}\frac{\mathrm{d}\ln(1-C)}{\mathrm{d}y}\right] \\ & - \left(\alpha_b^2 + \beta^2\right)\frac{\mathrm{d}^2\ln \mathrm{R}}{\mathrm{d}y^2}\hat{v}_{0b} \\ & + \frac{\mathrm{d}}{\mathrm{d}y}(\ln \mathrm{R}) \\ & \quad \times \left\{\left[\mathrm{D}^2 - \left(\alpha_b^2 + \beta^2\right) - \frac{\mathrm{d}}{\mathrm{d}y}(\ln \mathrm{R}) \cdot \mathrm{D}\right] - i\mathrm{R}(\alpha_b u_b - \omega_b)\right\} \\ & \times \left[-\frac{\mathrm{d}\hat{v}_{0b}}{\mathrm{d}y} - \hat{v}_{0b}\frac{\mathrm{d}}{\mathrm{d}y}\ln(1-C)\right] + \left(\alpha_b^2 + \beta^2\right)\left[\frac{\mathrm{d}}{\mathrm{d}y}(\ln \mathrm{R})\right]^2\hat{v}_{0b} \\ & + \left(\beta^2 + \alpha_b^2\right)\frac{\mathrm{d}\ln(1-C)}{\mathrm{d}y}\hat{v}_{0b}\frac{\mathrm{d}\ln \mathrm{R}}{\mathrm{d}y} = 0 \end{aligned} \tag{29}$$

4 Instability analysis for hyperconcentrated flow

Based on the equivalent viscosity coefficient model, Eq. (29) characterizing instability is not only related to the Reynolds and Froude numbers, and the wave number and frequency, but also to the specific density ρ_s/ρ, the reference concentration C_a, the suspension index ζ and the median diameter d_{50} as

$$f\left(\alpha_b, \beta, \omega_b, \mathsf{R}, \frac{\rho_s}{\rho}, C_a, \zeta, d_{50}\right) = 0 \tag{30}$$

4.1 *Uniformly-distributed sediment concentration*

If the sediment concentration is uniform, then $\mathsf{R} = \mathsf{R}_0(1 - C/2{d_{50}}^{1/2})$, in which $\mathsf{R}_0 =$ Reynolds number for clear water, such that Eq. (29) becomes

$$\left\{[\mathrm{D}^2 - (\alpha_b^2 + \beta^2)]^2 - i\mathsf{R}\left(1 - \frac{C}{2(d_{50})^{1/2}}\right)(\alpha_b u_b - \omega_b)\right.$$
$$\left.[\mathrm{D}^2 - (\alpha_b^2 + \beta^2)] + i\alpha_b\mathsf{R}\left(1 - \frac{C}{2(d_{50})^{1/2}}\right)\frac{\mathrm{d}^2 u_b}{\mathrm{d}y^2}\right\}\hat{v}_{0b} = 0 \tag{31}$$

and the instability relation reads

$$f(\alpha_b, \beta, \omega_b, \mathsf{R}_0, C_a, d_{50}) = 0 \tag{32}$$

Based on the above six factors when investigating instability, this study has found that: (1) compared with hyperconcentrated flows, instability in clear water is easier lost, (2) the 2D instability always occurs first in hyperconcentrated flows, (3) the sediment diameter has a significant effect on the instability. The following discussion details the above statements.

(1) In Eq. (31), if $C = 0$, the O-S equation governs the instability of clear water. The effect of sediment concentration on the instability contour and the critical (subscript *cr*) Reynolds number R_{cr} are shown in Fig. 4. If sediment concentration increases (Fig. 4a), the instability contour shifts towards the right side (i.e. larger R_{cr}). The contour shape looks similar for different concentrations, the lowest Reynolds number generating the instability loss always results for $\alpha_b \approx 1.05$. R_{cr} also increases with the sediment concentration C_a (Fig. 4b). Then, more energy is required to destabilize a flow, and thus the transition from stable to unstable flow becomes complicated and occurs at a higher R. It is therefore concluded that, if sediment concentration in water is uniform, the flow with a lower sediment concentration loses stability easier than with a higher concentration, and clear water loses instability easier than turbid water. The frequency at which the transition to instability occurs is, however, approximately the same for both clear and turbid water.

(2) With α and R as the 2D wave number and Reynolds number and using the Squire (1933) transformation, the 3D instability equation can be transformed to the corresponding 2D equation. The variation of the instability contour and the critical Reynolds number can then be computed with the wave number β along the transverse direction, where $\beta = 0$ corresponds to a 2D situation (Fig. 5). The critical number for the 2D instability is the lowest and the 2D instability always occurs first, therefore. Incorporating the findings of Bai and Luo (2002), and Bai and Xu (2005), the 2D ripples always form first on the alluvial bed and then evolve into 3D ripples for both clear and turbid water of uniform sediment concentration.

(3) As shown in Fig. 6, R_{cr} decreases with increasing median diameter. Within a certain range, the finer the sediment particle, the larger the total surface area of sediment. Therefore, the viscosity of turbid water of finer sediments is higher than that of coarser sediments, causing turbid water with fine sediments to be more stable.

4.2 *Exponentially-distributed sediment concentration*

Consider non-uniformly distributed sediment concentration, i.e. density and viscosity of the turbid water varies across the water

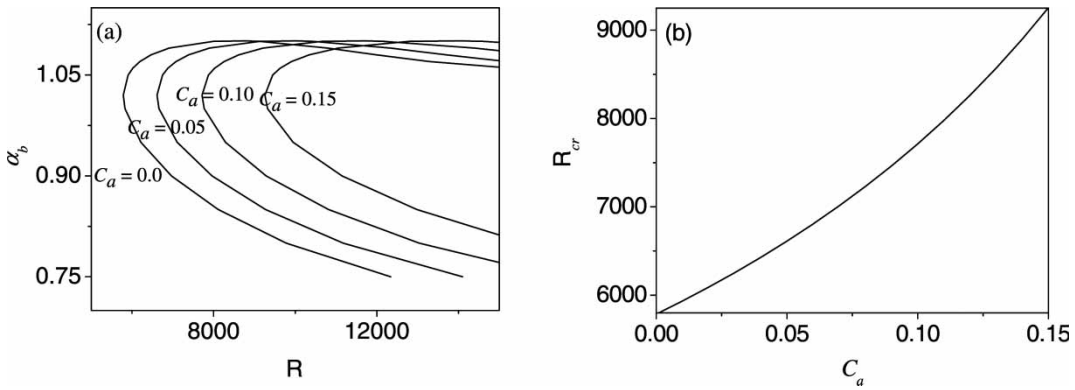

Figure 4 (a) Neutral curves $\alpha_b(\mathsf{R})$ for various sediment concentrations C_a, (b) variation of critical Reynolds number R_{cr} with sediment concentration C_a for ($d_{50} = 0.04$ mm, $\beta = 0$, $\rho_s = 2.63$ g/cm^3, $\rho = 1$ g/cm^3)

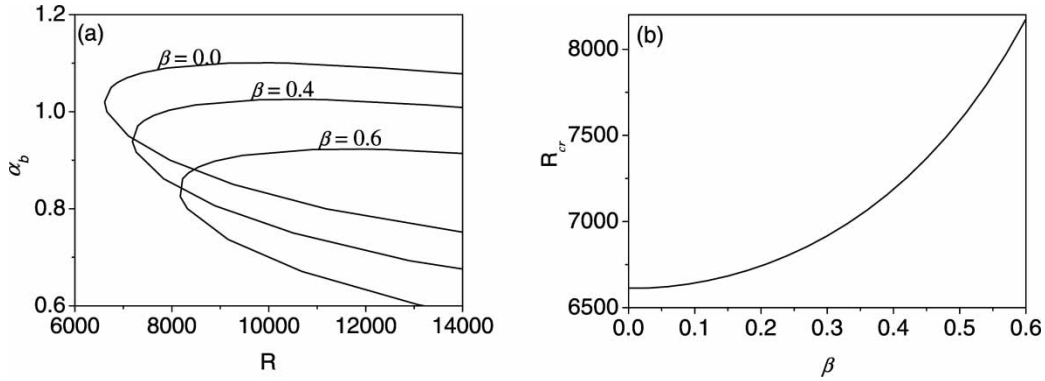

Figure 5 (a) Neutral curve for different wave numbers, (b) variation of R_{cr} with spread-direction wave number ($d_{50} = 0.04$ mm, $C_a = 0.0$, $\rho_s = 2.63$ g/cm^3, $\rho = 1.0$ g/cm^3)

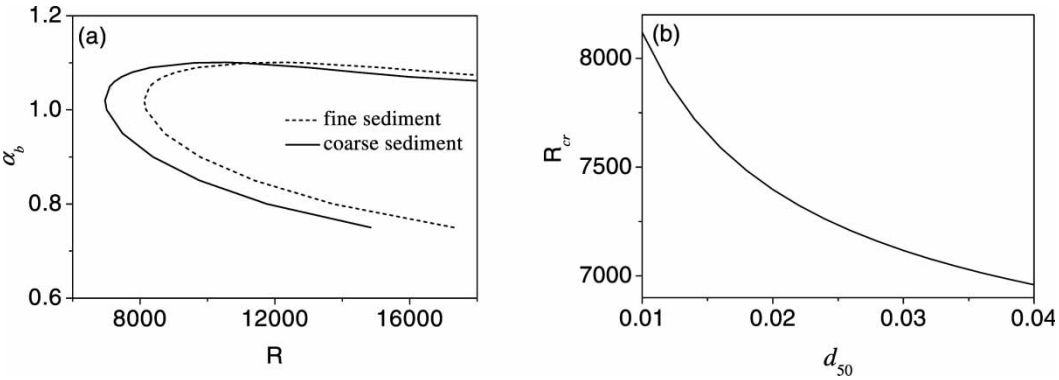

Figure 6 (a) Neutral curve for various medium diameters, (b) variation of medium diameter with R_{cr} ($d_{50} = 0.04$ mm, $\beta = 0.0$, $C_a = 0.0$, $\rho_s = 2.63$ g/cm^3, $\rho = 1.0$ g/cm^3)

depth. Substituting the exponentially-distributed sediment concentration by Eq. (19) and the corresponding velocity distribution Eq. (22) into the O-S equation (23). The latter is further discretized using the spectrum method and the Q-R decomposition to find the numerical results.

4.2.1 *Effect of distribution of sediment concentration on critical Reynolds number*

The suspension index ζ determines the distribution of sediment, as well as the variations of density and viscosity along the water depth. The non-uniform distribution of these properties causes the variation of characteristics of the instability for hyperconcentrated flows (Fig. 7). Figure 7(a) shows the instability contours associated with different suspension index ζ, where $\zeta = 0$ corresponds to the uniform sediment concentration. Higher ζ indicates faster increase of sediment concentration with water depth. Figure 7(a) shows that, with the same reference concentration C_a, the instability contour is not sensitive to the change of the suspension index.

Figure 7(b) shows the variation of the critical Reynolds number with the suspension index ζ, for different reference concentrations C_a. As expected, for clear water ($C_a = 0$), R_{cr} is not

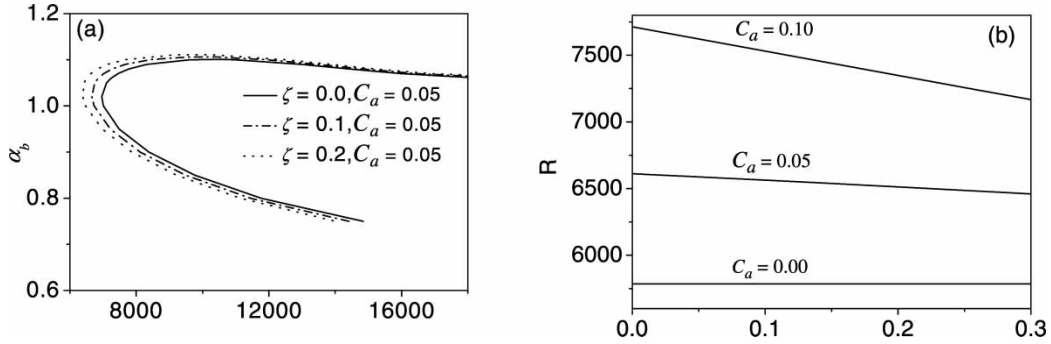

Figure 7 (a) Neutral curve for various suspension index, (b) variation of R_{cr} with suspension index ($d_{50} = 0.04$ mm, $\beta = 0.0$, $\rho_s = 2.63$ g/cm^3, $\rho = 1.0$ g/cm^3, $a = 0.0$)

related to ζ, and the critical Reynolds number is approximately 5785 with $\alpha_b = 1.02007$, in agreement with the results of the Poiseuille pipe flow (Orszag 1971), namely 5772 with $\alpha_b = 1.02056$. If $C_a \neq 0$, R_{cr} is very sensitive to changes in ζ, and decreases as ζ increases. This trend becomes more significant for higher C_a. Since the turbulent energy is mainly concentrated near the bed, the reference concentration C_a affects the stability within the laminar bed layer, as well as the generation, distribution and consumption of the turbulent energy.

4.2.2 *Effect of distribution of sediment concentration on flow instability*

If the sediment concentration is uniform, the Squire Transformation theoretically proves that the 2D instability always occurs first, as was supported from the present numerical results. However, if the sediment concentration is non-uniform, no relation between a 3D disturbance and the evolution of a 2D disturbance as well as its loss of stability can be theoretically derived. For non-uniform sediment concentration, a combined influence of the variations in the transverse wave number β, and the suspension index ζ on the characteristics of the stability was found. Figure 8 shows that, for identical C_a and ζ, R_{cr} increases with β; for constant β, R_{cr} decreases almost linearly with increasing ζ. In addition, the slope of the curves is approximately the same for different β. The critical Reynolds number for the 2D instability ($\beta = 0$) to occur is substantially lower than that for other β values, supporting the conclusion that the 2D instability always occurs first.

4.2.3 *Effect of sediment density on flow stability of hyperconcentrated flow*

In addition to the sediment concentration and its distribution, as well as the viscosity of the turbid water, the flow instability is also related to sediment density. Theoretically, it was found that the effect of density can be neglected. Figure 9 shows that the instability contours for both "light sand" ($\rho_s = 1.05$ g/cm^3) and "heavy sand" ($\rho_s = 2.63$ g/cm^3) almost collapse. The main effect of sediment on water is reflected from the interactions between them. Also, their interactions represent the counter-drag force of water to sediment and the counter-buoyancy of sediment to water. Consequently, sediment density has a small effect on hyperconcentrated flows, but it does not affect the Reynolds number as the major criterion determining the transition from laminar to turbulent flow, and thus is not a determinant factor.

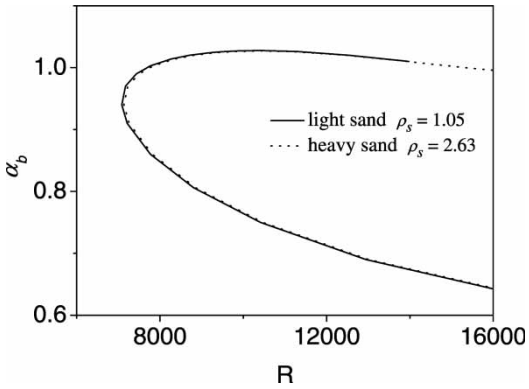

Figure 9 Variation of neutral curve for various sediment density ($d_{50} = 0.04$ mm, $a = 0.0$, $\rho = 1.0$ g/cm^3, $\zeta = 0.1$, $C_a = 0.05$, $\beta = 0.4$)

4.3 *Bingham characteristics of flow*

As mentioned above, the sediments of the Yellow River are largely derived from its middle reaches. Their sediment concentration is high, carrying not only coarse particles, but also a large amount of fine sediments. The sediment composition is widely distributed (Table 1). The equivalent viscosity coefficient model introduced by Sha (1961) was proved to be valid. However, it only gives reasonable results for loess (with $d \approx 0.02$ mm), but fails to reproduce the effect of sediment composition on the flow instability. Therefore, some of the results of the Bingham flow are given as a basis for comparison.

4.3.1 *Effect of sediment concentration on the Bingham hyperconcentration flow*

Frigaard *et al.* (1994) studied the stability characteristics of the linearized 2D disturbances of the plane Poiseuille flow of a

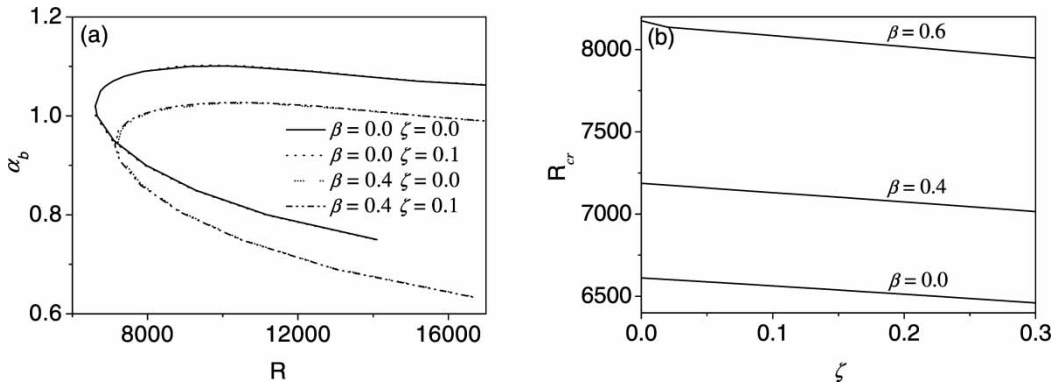

Figure 8 (a) Neutral curve under different three-dimensional wave number and suspend index, (b) variation of R_{cr} with suspend index ($d_{50} = 0.04$ mm, $\rho_s = 2.63$, $\rho = 1.0$, $a = 0.0$, $C_a = 0$)

Table 1 Composition characteristics of particles in middle and lower reaches of Yellow River

Station name	ρ_s (g/cm^3)	d_{50} (mm)	d_{90} (mm)	$d_{0.01}$ (mm)%	$\sum \Delta p_i/d_i$	C_{Vm}
Shen Mu	2.64	0.160	0.700	6	22	0.652
Sui De	2.69	0.050	0.092	9	38.8	0.602
Yan Chuan	2.66	0.035	0.070	22	70.6	0.550
Hua Xian	2.67	0.029	0.100	20	70.5	0.550
Tong Guan	2.65	0.022	0.075	29	110.7	0.511
Da Ning	2.70	0.030	0.070	26	134.6	0.494
Da Cun	2.70	0.023	0.060	28	140	0.491
Ding Jia Gou	2.70	0.034	0.074	17	140	0.491
Hua Yuan Kou	2.66	0.005	0.035	70	700	0.351

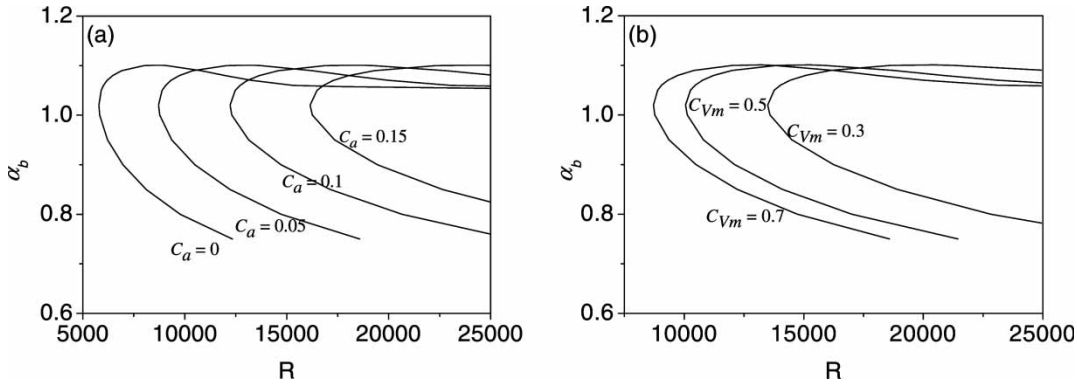

Figure 10 (a) Neutral curves for various sediment concentrations ($C_{Vm} = 0.7$), (b) effect of critical concentration ($C = 0.05$)

Bingham fluid, which exhibit a yield stress in addition to a plastic viscosity by deriving the O-S equation, which may be expressed as the open channel flow as

$$\left\{\left[\mathrm{D}^2-\alpha^2\right]^2-i\mathrm{R}_0\left\{1-\left[1+\frac{3}{2}\left(\frac{C_{Vm}-C}{C_{Vm}}\right)^4\right]\frac{C}{C_{Vm}}\right\}^{2.5}(\alpha u_b-\omega)\right.$$
$$\left.\times\left(\mathrm{D}^2-\alpha^2\right)\right.$$
$$+i\alpha\mathrm{R}_0\left\{1-\left[1+\frac{3}{2}\left(\frac{C_{Vm}-C}{C_{Vm}}\right)^4\right]\frac{C}{C_{Vm}}\right\}^{2.5}\frac{\mathrm{d}^2u_b}{\mathrm{d}y^2}\Bigg\}\hat{v}_{0a}$$
$$-4\alpha^2\mathrm{B}\mathrm{D}\left(\frac{\mathrm{D}\hat{v}_{0a}}{|\mathrm{D}u_b|}\right)=0 \qquad (33)$$

$$\hat{v}_{0a}=0 \quad \mathrm{D}\hat{v}_{0a}=0 \quad \text{at} \quad y=0 \quad \hat{v}_{0a}=0 \quad \mathrm{D}\hat{v}_{0a}=0$$
$$\mathrm{D}^2\hat{v}_{0a}=\frac{\mathrm{B}h}{1-y*} \quad \text{at} \quad y=y*.$$

The effects of sediment diameter and sediment size distribution are accounted for by the critical concentration. Obviously, for identical sediment characteristics, the larger the medium diameter, the higher becomes the critical concentration. Also, for the same medium diameter, the wider the size distribution, the lower is the critical concentration. Note from Fig. 10 that stability decreases with the critical concentration. On the one hand, these results confirm the discussion of Fig. 5 that the instability of hyperconcentrated flow increases as the medium diameter decreases. On the other hand, if the particle size distribution is wide, the pores between the coarse particles are filled by finer particles and the coarse particles are surrounded by a bound water layer. Its effect on the viscosity coefficient then reduces.

5 Conclusions

For clear water as a Newtonian fluid, the transition from laminar to turbulent flow is controlled by the ratio of inertia force to viscous forces, i.e. the Reynolds number. For hyperconcentrated flow as a non-Newtonian fluid, the factors controlling this transition are quite different, including sediment concentration, the distribution of sediment concentration, viscous coefficient of turbid water, as well as the particle diameter. Similar to clear water, the loss of stability for a hyperconcentrated flow occurs first in a 2D state then evolving into a 3D form. Regardless of clear or turbid water, 2D ripples always occur on the bed first, and then evolve into 3D ripples, in agreement with actual field observations and laboratory experiments. The instability occurs more easily in clear than in turbid water. Also, water of low sediment concentration loses stability easier than of higher concentration. The critical Reynolds number increases with the sediment concentration. For hyperconcentrated flows, the finer the sediments, the higher the turbid viscous coefficient.

Consequently, with the same sediment concentration, the turbid water with fine sediments is more stable than with coarse sediments.

Two main parameters characterize the sediment concentration, i.e. reference concentration near the bed and the suspension index describing the distribution of sediment concentration. The reference concentration significantly affects flow instability. Not only does it change the critical Reynolds number, which increases with sediment concentration, but also changes the sensitivity of the critical Reynolds number to the suspension index. The suspension coefficient has less effect; the critical Reynolds number decreases slowly as the suspension coefficient increases, indicating that the turbulent energy is concentrated near the bed, and the presence of the hyperconcentrated flow above it affects the characteristics of the flow stability. In addition, it was found that the effect of sediment density on the flow stability is negligible, because sediment density does not affect the key parameters controlling the transition from laminar to turbulent flow, i.e. the critical Reynolds number of hyperconcentrated open-channel flow.

The critical concentration depends on the sediment diameter and the size composition. Under otherwise identical conditions, the increase of the medium sediment diameter or a narrower range of the size distribution increase the critical concentration, and further cause the flow to become unstable faster. The results confirm the present conclusions, and also illustrate that the effect of the combined water layer on the viscosity coefficient becomes less important if the pores between the coarse particles are filled by finer particles and the coarse particles are surrounded by a combined water layer.

Acknowledgements

This project was supported by the National Natural Science Foundation of China, Grant No. 50809045, 50979066 and 40776045, and the 973 program (2007CB714101).

Notation

C = volumetric sediment concentration
d = sediment diameter (m)
F = Froude number (–)
g = gravity acceleration (m/s^2)
h = water flow depth (m)
J = bottom slope (–)
p = pressure ($kg/m/s^2$)
R = Reynolds number
U, V, W = non-dimensional velocities in x, y, z directions, respectively (–)
α_b = wave number in x direction (–)
β = wave number in z direction (–)
δ = thickness of pellicular zone (m)
Δp_i = percentage of ith sediment (–)
ζ = sediment suspension index (–)
μ_e = equivalent viscosity coefficient (kg/m/s)
μ_0 = viscosity coefficient of clear water (kg/m/s)
τ_{ij} = stress components of the flow (N/m^2)

Subscripts

e = equivalent
0 = clear water
ij = different direction, like x, y, z directions

References

Abulnaga, B.E. (2002). *Slurry systems handbook*. McGraw-Hill, New York.

Alderman, N.J., Haldenwang, R. (2007). A review of Newtonian and non-Newtonian flow in rectangular open channels. *Hydrotransport* Cape Town 17, 87–106.

Bai, Y.C., Luo, J.S. (2002). The loss of stability of laminar flow in open channel and the mechanism of sand ripple formation. *Applied Mathematics and Mechanics* 23(3), 254–268.

Bai, Y.C., Ng, C.O., Shen, H.T., Wang, S.Y. (2002). Rheological properties and incipient motion of cohesive sediment in the Haihe Estuary of China. *China Ocean Engineering* 16(4), 483–498.

Bai, Y.C., Xu, H.J. (2005). A study on the stability of laminar open-channel flow over a sandy ripples bed. *Science in China* Ser. E 48(1), 83–103.

Chien, N., Wan, Z.H., McNown, J.S. (1998). *Mechanics of sediment movement*. ASCE Press, New York.

Fei, X.J. (1994). *The deliver dynamics of thick liquid and granular materials*. University Press, Tsinghua [in Chinese].

Fei, X.J., Yang, M.Q. (1985). The physical properties of flow with hyperconcentration of sediment. Proc. Intl. Workshop *Flow at Hyperconcentrations of Sediment*, IRTCES, Beijing, China, 296–308.

Frigaard, I.A., Howison, S.D., Sobey, I.J. (1994). On the stability of Poiseuille flow of a Bingham fluid. *J. Fluid Mech*. 263, 133–150.

Frigaard, I.A., Nouar, C. (2003). On three-dimensional linear stability of Poiseuille flow of Bingham fluids. *Phys. Fluids* 15(10), 2843–2851.

Hanks, R.W. (1963). The laminar-turbulent transition for fluids with a yield stress. *AIChE J*. 9(3), 306–309.

Hurst, H.E. (1929). The suspension of sand in water. *Proc.Royal Soc.* London A 124, 196–201.

Julien, P.Y. (1989). Laboratory analysis of hyper-concentrations Proc. Intl. Symp. *Sediment Transport Modeling* New Orleans, 681–686. ASCE, New York.

Julien, P.Y., Lan, Y.Q. (1991). Rheology of hyper-concentrations. *J. Hydraulic Eng*. 115(3), 346–353.

Kobayashi, N., Seo, N.S. (1985). Fluid and sediment interaction over a plane bed. *J. Hydraulic Eng*. 111(6), 903–921.

Lane, E.W., Kalinske, A.A. (1941). Engineering calculation of suspended sediment. *Trans. Amer. Geophs. Union* 603–607.

Nouar, C., Frigaard, I. (2001). Nonlinear stability of Poiseuille flow of a Bingham fluid: Theoretical results and comparison with phenomenological criteria. *J. Non-Newtonian Fluid Mech*. 100, 127–149.

O'Brien, J.S., Julien, P.Y. (1995). Physical properties and mechanics of hyper-concentrated sediment flows. Proc. ASCE Specialty Conf. *Delineation of Landslide, Flash Flood and Debris Flow Hazards in Utah*, 1985 Utah Water Research Lab, Series UWRL/C-85103, 260–279.

Orszag, S.A. (1971). Accurate solution of Orr-Sommerfeld stability equation. *J. Fluid Mech*. 50, 689–703.

Qian, N. (1989). *Movement of hyper-concentrated flow.* University Press, Tsinghua [in Chinese].

Qian, N., Zhang, R., Wan, Z., Wang, X. (1985). The hyper-concentrated flow in the main stem and tributaries of the Yellow River. Proc. Intl. Workshop *Flow at Hyper-concentrations of Sediment*. Beijing III(4), 1–15.

Roscoe, R. (1952). The viscosity of suspensions of rigid sphere. *Bri. J. Applied Phys*. 3, 262–269.

Squire, H.B. (1933). On the stability for three-dimensional disturbances of viscous fluid flow between parallel wall. *Proc. Roy. Soc*. London A 142, 621–628.

Sha, Y.Q. (1961). *Introduction to river mechanics*. Shanxi Science Technology Press, Xi'an [in Chinese].

Thomas, D.G. (1965). Transport characteristics of suspensions, Pt. VIII A note on the viscosity of Newtonian suspensions of uniform spherical particles. *J. Colloid Sci.* 20, 267–277.

Wan, Z., Wang, Z.Y. (1994). *Hyper-concentrated flow.* IAHR Monograph Series. Balkema, Rotterdam.

Wang, Z.Y. (2002). Free surface instability of non-Newtonian laminar flows. *J. Hydraulic Res*. 40(4), 449–460.

Wang, Z.Y., Larsen, P., Nestmann, F., Dittrich, A. (1998). Resistance and drag reduction of hyper-concentrated flows over rough boundaries. *J. Hydraulic Eng*. 121(1), 1–9.

Wang, Z.Y., Larsen, P., Xiang, W. (1994). Rheological properties of sediment suspensions and their implications. *J. Hydraulic Res*. 32(4), 495–516.

Wang, Z.Y., Qian, N. (1985). A preliminary investigation on the mechanism of hyper-concentrated flow. Proc. Intl. Workshop *Flow at Hyper-concentrations of Sediment* Beijing II(4), 1–20.

Wasp, E.J. (1977). *Solid-liquid flow of slurry pipeline transportation*. Gulf, Houston.

Zhao, W.L., Zhang, H.W., Pan, X.D., Miu, F.J. (1997). sediment in Yellow River. Yellow River Conservancy Press, Henan Province [in Chinese].